RIS Meets Aerodynamic HAPS: A Multi-Objective Optimization Approach

Arman Azizi, *Student Member, IEEE*, and Arman Farhang, *Senior Member, IEEE*

***Abstract*—In this letter, we propose a novel network architecture for integrating terrestrial and non-terrestrial networks (NTNs) to establish connection between terrestrial ground stations which are unconnected due to blockage. We propose a new network framework where reconfigurable intelligent surface (RIS) is mounted on an aerodynamic high altitude platform station (HAPS), referred to as aerodynamic HAPS-RIS. This can be one of the promising candidates among non-terrestrial RIS (NT-RIS) platforms. We formulate a mathematical model of the cascade channel gain and time-varying effects based on the predictable mobility of the aerodynamic HAPS-RIS. We propose a multi-objective optimization problem for designing the RIS phase shifts to maximize the cascade channel gain while forcing the Doppler spread to zero, and minimizing the delay spread upper bound. Considering an RIS reference element, we find a closed-form solution to this optimization problem based on the Pareto optimality of the aforementioned objective functions. Finally, we evaluate and show the effective performance of our proposed closed-form solution through numerical simulations.**

***Index Terms*—RIS, NTNs, HAPS, 6G, time-varying channel.**

I. Introduction

ONE OF the most important targets in sixth generation wireless networks (6G) is the provision of ubiquitous connectivity. This aim can be attained by integration of terrestrial and non-terrestrial networks (NTNs), [1]. To this end, reconfigurable intelligent surface (RIS) can be exploited to boost the channel gain by creating a multi-path environment. Non-terrestrial RIS (NT-RIS) is an intelligent intermediate reflection layer, where RIS is mounted on a non-terrestrial platform to connect the unconnected terrestrial infrastructures. Extensive research has been conducted to address the benefits of adopting NT-RIS in wireless networks, see [2], [3], [4], [5] and the references therein. In practical cases, high altitude platform station (HAPS)-RIS is one of the promising candidates to be exploited for NT-RIS compared to other non-terrestrial platforms such as satellite-RIS and unmanned aerial vehicle (UAV)-RIS, [4], [5]. HAPS operates at much higher altitude which leads to establishing line of sight (LoS) dominated connection and a much wider coverage area compared to UAV. Furthermore, HAPS is much larger than UAV so that RIS with a large number of elements can be mounted on it [2], [4]. The advantages of exploiting RIS over relay is well articulated in [2], e.g., lower-cost, simpler hardware, shorter transmission delay, less power consumption, and longer communication duration. In [6], the authors prove that if the RIS is large enough it can beat the relay in terms of energy-efficiency. Due to the large size of HAPS, large number of RIS elements can be mounted on HAPS, and hence, RIS is the better option. Even if a large number of RIS elements are deployed, the HAPS's payload is light due to the thin and lightweight materials from which the RIS elements are manufactured [2]. From the perspective of HAPS mobility, there are two types of HAPSs, aerostatic and aerodynamic, [7]. The investigation of HAPS-RIS communications is still in its infancy. The existing literature on this topic is mostly focused on aerostatic HAPS-RIS, [4], [5], [8], [9], while the aerodynamic HAPS-RIS is left as an open research topic. The necessity of research on this direction has been emphasised in [10]. The advantages of exploiting aerodynamic over aerostatic HAPS in wireless networks are well articulated in [7], e.g., low-cost and swift deployment, and high resilience to turbulence. These features make aerodynamic HAPS a promising candidate technology in the move towards integration of terrestrial and non-terrestrial networks, [7]. However, high mobility of aerodynamic HAPS leads to time-varying channel effects. Accordingly, the main research question that arises is "*Can aerodynamic HAPS-RIS bring connectivity to the unconnected ground stations in presence of time-varying channel?*".

There exist a number of works in the literature that consider RIS-based networks in the presence of time-varying channel, which can be classified into two groups where RIS is fixed, [11], [12], [13], or mobile, [14], [15], [16]. Our proposed network architecture in this letter falls under the area of the latter one, where the RIS is mobile. In [14] and [15], the authors present efficient Doppler shift mitigation methods, including transmission protocol and RIS phase shift control, where both of RIS and user equipment are deployed in a high-mobility terrestrial vehicle. The main difference between [14] and [15], is the design of the transmission protocol. In [16], the authors present a cooperative passive beamforming and distributed channel estimation to maximize the overall channel gain between an RIS-aided low-earth orbit satellite and a ground node. While the main focus of [14], [15], [16] is channel estimation, to the best of our knowledge, there is no existing work which geometrically formulates all the channel metrics and time-varying effects based on predictive mobility of RIS, which can play a vital role in reducing the computational complexity. Furthermore, the authors in [14], [15], [16] only consider one side of the cascade channel to be time-varying, while in this letter we investigate the case where both sides of the cascade channel are time-varying.

To summarize, this letter addresses the aforementioned gaps in the literature with the ensuing contributions: (i) We introduce a *novel network architecture* for NT-RIS assisted networks. We propose a new system model where RIS is mounted on aerodynamic HAPS to connect the unconnected terrestrial ground stations in emergency situations thanks to

Manuscript received 2 May 2023; revised 17 June 2023; accepted 6 July 2023. Date of publication 17 July 2023; date of current version 9 November 2023. This work was supported in part by the Science Foundation Ireland under Grant 18/CRT/6222, Grant 13/RC/2077_P2, Grant 19/FFP/7005(T), and Grant 21/US/3757. The associate editor coordinating the review of this article and approving it for publication was K. Wang. *(Corresponding author: Arman Azizi.)*

The authors are with the Department of Electronic and Electrical Engineering, Trinity College Dublin, Dublin, D02 PN40 Ireland (e-mail: azizia@tcd.ie; arman.farhang@tcd.ie).

Digital Object Identifier 10.1109/LWC.2023.3296023

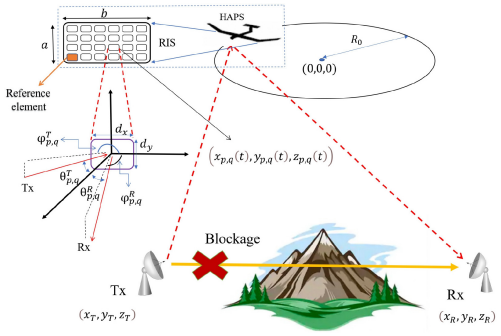

Fig. 1. Proposed network architecture based on aerodynamic HAPS-RIS.

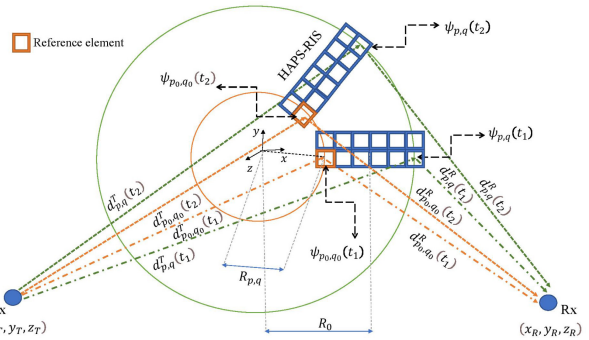

Fig. 2. Geometrical mobility pattern of RIS elements based on the predictable mobility of the aerodynamic HAPS.

significant features of aerodynamic HAPS. (ii) We *mathematically model the mobility pattern of each RIS element* based on the dimensions of the RIS and the RIS elements, and the predictive trajectory of the aerodynamic HAPS-RIS. Next, we obtain a geometrical model for all the channel metrics and time-varying effects. To the best of our knowledge, there is no work which geometrically models the mobility profile of a mobile RIS based on these parameters. (iii) We propose a multi-objective optimization problem in which the objective functions are the channel gain, the delay spread upper bound and the Doppler spread. We *obtain a closed-from solution* for the RIS phase shifts, by introducing a reference RIS element, adopting Pareto optimality. The obtained closed-form is based on the known locations of Tx and Rx, and the known time-varying position of the aerodynamic HAPS-RIS, thanks to knowing its mobility pattern. This leads to practical and simple implementation as the RIS phase shifts can be efficiently calculated by the onboard processing unit on HAPS.

II. System Model and Problem Formulation

In this letter, we consider a heavy blockage scenario where the link between the terrestrial transmitter (Tx) and receiver (Rx) is blocked. We consider the network architecture in Fig. 1, exploiting aerodynamic HAPS-RIS to connect the unconnected ground stations. We consider the RIS to be a rectangle with the length a and the width b, which is located on the bottom of the HAPS in the xy-plane. d_x and d_y are the dimensions of each RIS element, which are in the range of $[\frac{\lambda_c}{10}, \frac{\lambda_c}{5}]$ where $\lambda_c = \frac{c_0}{f_c}$ is the carrier wavelength [17]. f_c is the carrier frequency and c_0 is the speed of light. The RIS consists of $P = \lceil \frac{a}{d_x} \rceil$ columns and $Q = \lceil \frac{b}{d_y} \rceil$ rows of reflecting elements. The aerodynamic HAPS has a circular movement in the stratosphere with radius R_0 centered at the origin of the Cartesian coordinate system and the velocity v. It is not practical to consider different trajectories for the aerodynamic HAPS, like what is expected for UAVs. It is vital to consider the circular trajectory for the aerodynamic HAPS, which leads to quasi-stationary position, that brings resilience to turbulence [7]. As the aerodynamic HAPS is moving with high speed, both sides of the cascade channel for each RIS element are time-varying. This can be clearly observed in Fig. 2 which shows the geometrical mobility pattern of RIS elements based on the predictive mobility of the aerodynamic HAPS.

Definition 1: The geometrical mobility pattern of the RIS elements can be attained as a function of the predictive mobility of the aerodynamic HAPS, and the dimensions a, b, d_x, and d_y as $(x_{p,q}(t), y_{p,q}(t), z_{p,q}(t)) = (R_{p,q}\cos(\frac{vt}{R_{p,q}} + \alpha_{p,q}), R_{p,q}\sin(\frac{vt}{R_{p,q}} + \alpha_{p,q}), 0)$ where

$$R_{p,q} = \sqrt{(R_0 - \frac{a}{2} + (p - \frac{1}{2})d_x)^2 + (-\frac{b}{2} + (q - \frac{1}{2})d_y)^2}, \tag{1}$$

$$\alpha_{p,q} = \arctan\left(\frac{-\frac{b}{2} + (q - \frac{1}{2})d_y}{R_0 - \frac{a}{2} + (p - \frac{1}{2})d_x}\right). \tag{2}$$

We consider a LoS dominated scenario for the links between Tx/Rx and HAPS-RIS as the aerodynamic HAPS-RIS flies in a high altitude, i.e., 20 km [7]. Furthermore, in HAPS-RIS scenarios, the ground stations are considered as high directional antenna gain transceivers which leads to establishing strong and dominant LoS link [8], [9]. The Tx sends a passband signal $s_p(t) = \sqrt{2}\Re\{s(t)\ \exp(j2\pi f_c t)\} = \frac{s(t)\ \exp(j2\pi f_c t) + s^*(t)\ \exp(-j2\pi f_c t)}{\sqrt{2}}$ where $s(t)$ is the complex baseband signal with bandwidth $B/2$ which is modulated to the carrier frequency f_c satisfying $B \ll 2f_c$, [18]. Thus, the received baseband signal can be shown as $r(t) = \sum_{p=1}^{P}\sum_{q=1}^{Q}\Gamma_{p,q}(t)\exp(-j2\pi f_c \tau_{p,q}(t) - j\psi_{p,q}(t))s(t - \tau_{p,q}(t) - \frac{\psi_{p,q}(t)}{2\pi f_c}) + n(t)$ where $\Gamma_{p,q}(t)$ is the cascade channel gain coefficient for the RIS element (p, q) and $n(t)$ is the additive white Gaussian noise (AWGN). Additionally, $\psi_{p,q}(t)$ is the phase shift of the RIS element (p, q). Using the Friis model, [19], $\Gamma_{p,q}(t)$ is the multiplication of the ground to air and air to ground amplitude gains as

$$\Gamma_{p,q}(t) = \frac{\lambda_c^2}{16\pi^2 \prod_S d_{p,q}^S(t)} \sqrt{\prod_S g_S^{p,q}(t) \prod_S g_{p,q}^S(t)}, \tag{3}$$

where $S \in \{\mathrm{T}, \mathrm{R}\}$ represents the Tx/Rx. The distance between the RIS element (p, q) and the Tx/Rx can be calculated as $d_{p,q}^S(t) = \sqrt{(x_{p,q}(t) - x_S)^2 + (y_{p,q}(t) - y_S)^2 + (z_{p,q}(t) - z_S)^2}$.

Moreover, $g_{p,q}^S(t)$ is the antenna gain of RIS element (p, q) to S, which can be a function of $\theta_{p,q}^S(t) \in [0, \pi]$ and $\varphi_{p,q}^S(t) \in [0, 2\pi]$. We consider that $g_{p,q}^S(t)$ is zero for $\theta_{p,q}^S(t) \in [\frac{\pi}{2}, \pi]$. The term $\theta_{p,q}^S(t) = \arccos(\frac{z_S - z_{p,q}(t)}{d_{p,q}^S(t)})$ is the elevation angle from the RIS element (p, q) to S. The term $\varphi_{p,q}^S(t) = \arctan(\frac{y_S - y_{p,q}(t)}{x_S - x_{p,q}(t)})$ is the azimuth angle from the RIS element (p, q) to S. Furthermore, $g_S^{p,q}(t)$ is the antenna gain of the Tx/Rx to/from the RIS element (p, q). The terms $\theta_S^{p,q}(t)$ and $\varphi_S^{p,q}(t)$ are the angle of elevation and azimuth

from S to the RIS element (p, q), respectively. $\tau_{p,q}(t)$ is the cascade path delay for the RIS element (p, q), which can be formulated as $\tau_{p,q}(t) = \frac{\sum_S d^S_{p,q}(t)}{c_0}$.

The instantaneous cascade channel gain as the ratio between the received power, $P_{\mathrm{R}}(t)$, and the time-invariant transmit power, P_{T}, can be obtained as

$$\frac{P_{\mathrm{R}}(t)}{P_{\mathrm{T}}} = \left| \sum_{p=1}^{P} \sum_{q=1}^{Q} \Gamma_{p,q}(t) \exp(-j2\pi f_{\mathrm{c}} \tau_{p,q}(t) - j\psi_{p,q}(t)) \right|^2, \tag{4}$$

The time-varying effects caused by the cascade paths through the RIS elements, i.e., the Doppler spread, $B_{\mathrm{Do}}(t)$, and the delay spread, $T_{\mathrm{De}}(t)$, can be obtained as [13], [18]

$$B_{\mathrm{Do}}(t) = f_{\mathrm{c}} \times \max_{p,q,p',q'} \left| \frac{d}{dt}(\tau_{p,q}(t) + \frac{\psi_{p,q}(t)}{2\pi f_{\mathrm{c}}}) - \frac{d}{dt}(\tau_{p',q'}(t) + \frac{\psi_{p',q'}(t)}{2\pi f_{\mathrm{c}}}) \right|, \tag{5}$$

$$T_{\mathrm{De}}(t) = \max_{p,q}\{\tau_{p,q}(t) + \frac{\psi_{p,q}(t)}{2\pi f_{\mathrm{c}}}\} - \min_{p,q}\{\tau_{p,q}(t) + \frac{\psi_{p,q}(t)}{2\pi f_{\mathrm{c}}}\}. \tag{6}$$

We consider a multi-objective optimization problem, including analogous objective functions as in [13], to maximize (4) while minimizing (5) and (6) simultaneously. Therefore, the main optimization problem can be formulated as

$$\mathrm{OP}: \max_{\forall p,q,t:\ \psi_{p,q}(t) \geq 0} \left[\frac{P_{\mathrm{R}}(t)}{P_{\mathrm{T}}}, -B_{\mathrm{Do}}(t), -T_{\mathrm{De}}(t) \right]. \tag{7}$$

The feasible set $\psi_{p,q}(t) \geq 0$, originates from the causality requirement [18]. We consider a mobile RIS where both sides of the cascade channel are time-varying while in [13] the RIS is fixed and only one side of the cascade channel is time-varying. Furthermore, we consider the link between Tx and Rx is blocked while in [13] the direct link is available. The adopted technique in [13] does not work for our proposed model to solve OP. To tackle this issue, as can be seen in Fig. 2, we consider a single RIS element as a reference with variable phase shift $\psi_{p_0,q_0}(t)$, so that the other phase shifts can be obtained based on that. The cascade path through the reference element is called reference path.

III. Proposed RIS Phase Shift Design

To find the optimal solution of OP, let us consider the search space as the set $\mathbf{\Psi}$. Even if we relax the continuous RIS phase shifts to discrete ones with M quantization levels, to simplify the problem, the search space has M^{PQ} states. As this is a massive number for a large number of RIS elements, finding the optimal solution is intractable in terms of computational complexity. For large values of M, to get close to the continuous case, the search space $\mathbf{\Psi}$ becomes prohibitively large. Thus, it is evident that if the phase shifts are continuous like our proposed scenario, solving (7) is not affordable in terms of computational complexity. To tackle this issue, we find the Pareto optimal solution of OP in *Proposition 1* by decomposing OP into $\mathrm{OP_1}$ and $\mathrm{OP_2}$.

Proposition 1: Let us decompose OP into $\mathrm{OP_1}$ and $\mathrm{OP_2}$ as

$$\mathrm{OP_1}: \forall p, q, t: \psi_{p,q}(t) \in \arg\max_{\mathbf{\Psi}} \frac{P_{\mathrm{R}}(t)}{P_{\mathrm{T}}} \cap \arg\min_{\mathbf{\Psi}} B_{\mathrm{Do}}(t), \tag{8}$$

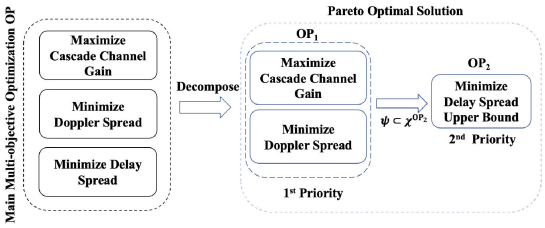

Fig. 3. The proposed Pareto Optimal Solution Method.

$$\mathrm{OP_2}: \forall p, q, t: \psi_{p,q}(t) \in \arg\min_{\boldsymbol{\psi} \subset \boldsymbol{\chi}^{\mathrm{OP_2}}} T^{\mathrm{upp}}_{\mathrm{De}}(t). \tag{9}$$

As $\mathrm{OP_1}$ and $\mathrm{OP_2}$ can not be optimized simultaneously, we consider that $\mathrm{OP_1}$ has the higher priority order compared to $\mathrm{OP_2}$, which is elaborated later in *Lemma 2*. As can be seen in Fig. 3, $\mathrm{OP_1}$ optimizes $\frac{P_{\mathrm{R}}(t)}{P_{\mathrm{T}}}$ and $B_{\mathrm{Do}}(t)$ simultaneously. Let us consider all the possible solutions of $\mathrm{OP_1}$ is the solution set $\boldsymbol{\chi}^{\mathrm{OP_2}}$ which is a feasible set for $\mathrm{OP_2}$. In $\mathrm{OP_2}$, we optimize the delay spread upper bound, $T^{\mathrm{upp}}_{\mathrm{De}}(t)$, over the feasible set $\boldsymbol{\psi} \subset \boldsymbol{\chi}^{\mathrm{OP_2}}$ resulting from solving $\mathrm{OP_1}$. The Pareto optimal closed-form solution of (7) is

$$\psi_{p,q}(t) = 2\pi \mathrm{mod}\big(f_{\mathrm{c}}\big(\tau_{p_0,q_0}(t) - \tau_{p,q}(t)\big), 1\big), \tag{10}$$

where $\mathrm{mod}(\mu, \eta)$ is the remainder of the division of μ by η. $\tau_{p_0,q_0}(t)$ is the delay spread through the RIS reference element. There is no need to consider $\psi_{p,q}(t) \leq 2\pi$ as it is already satisfied in our closed-form solution.

Proof: The Pareto optimal solution can be attained based on lemma 1 and 2. ∎

Lemma 1: As the Doppler spread, $B_{\mathrm{Do}}(t)$ in (5), is a function of RIS phase shifts, using the following criterion in RIS phase shift design, this effect becomes zero.

$$\frac{d}{dt}\psi_{\tilde{p},\tilde{q}}(t) = \frac{d}{dt}\psi_{p_0,q_0}(t) + 2\pi f_{\mathrm{c}} \frac{d}{dt}\varpi_{\tilde{p},\tilde{q}}(t), \tag{11}$$

where $\varpi_{\tilde{p},\tilde{q}}(t) = \tau_{p_0,q_0}(t) - \tau_{\tilde{p},\tilde{q}}(t)$. For brevity, RIS elements except the reference element are shown as $(\tilde{p}, \tilde{q})$.

Proof: The Doppler spread can be represented as

$$B_{\mathrm{Do}}(t) = \max\{B_{\mathrm{Do},1}(t), B_{\mathrm{Do},2}(t)\}, \tag{12}$$

where the Doppler spread between the reference path and other cascade paths is

$$B_{\mathrm{Do},1}(t) = f_{\mathrm{c}} \max_{\tilde{p},\tilde{q}} \Big| \frac{d}{dt}(\tau_{\tilde{p},\tilde{q}}(t) + \frac{\psi_{\tilde{p},\tilde{q}}(t)}{2\pi f_{\mathrm{c}}}) - \frac{d}{dt}(\tau_{p_0,q_0}(t) + \frac{\psi_{p_0,q_0}(t)}{2\pi f_{\mathrm{c}}}) \Big|, \tag{13}$$

and the Doppler spread between the cascade paths except reference path is

$$B_{\mathrm{Do},2}(t) = f_{\mathrm{c}} \max_{\tilde{p},\tilde{q},\tilde{p}',\tilde{q}'} \Big| \frac{d}{dt}(\tau_{\tilde{p},\tilde{q}}(t) + \frac{\psi_{\tilde{p},\tilde{q}}(t)}{2\pi f_{\mathrm{c}}}) - \frac{d}{dt}(\tau_{\tilde{p}',\tilde{q}'}(t) + \frac{\psi_{\tilde{p}',\tilde{q}'}(t)}{2\pi f_{\mathrm{c}}}) \Big|. \tag{14}$$

In order to make the Doppler spread zero, we force both $B_{\mathrm{Do},1}$ and $B_{\mathrm{Do},2}$ to zero, which leads to (11). ∎

Lemma 2: The Pareto optimal solution, (10), optimizes (4) and (5) simultaneously, and after that minimizes $T^{\mathrm{upp}}_{\mathrm{De}}(t)$.

Proof: After forcing Doppler spread to zero, we have a feasible set for $\psi_{p,q}(t)$ based on (11). First, we integrate (11) with

respect to t and substitute the result into (4). In the next step, in order to maximize the instantaneous cascade channel gain, all the terms of (4) should have the same phase. Therefore, $\forall p, q$ choosing

$$\psi_{p,q}(t) = \begin{cases} \psi_{p_0,q_0}(t) & p = p_0, q = q_0, \\ 2\pi f_c \varpi_{\tilde{p},\tilde{q}}(t) + 2\pi\zeta_{\tilde{p},\tilde{q}}(t) + \psi_{p_0,q_0}(t) & \text{Otherwise}, \end{cases} \tag{15}$$

and $\zeta_{\tilde{p},\tilde{q}}(t) \in \mathbb{Z}$, maximize (4). It is clear that (4) is the most important metric among the objective functions, which leads to maximizing signal-to-noise ratio. From (11) and (15), we see that (4) and (5) can be simultaneously optimized, irrespective of the phase shift $\psi_{p_0,q_0}(t)$. Due to the causality requirement, $\psi_{p,q}(t) \geq 0$, we can attain the upper bound of delay spread based on (6) as

$$T_{\text{De}}^{\text{upp}}(t) = \max_{p,q}\{\tau_{p,q}(t) + \frac{\psi_{p,q}(t)}{2\pi f_c}\} - \min_{p,q}\{\tau_{p,q}(t)\}. \tag{16}$$

From (15) and (16), it is obvious that there is no single solution for optimizing $\text{OP}_\mathbf{1}$ and $\text{OP}_\mathbf{2}$ simultaneously. As (16) is an increasing function in $\psi_{p,q}(t)$, zero phase shift is needed $\forall p, q, t$ to minimize (16), which is impossible according to (15). Instead, there are infinite non-inferior solutions, [20]. By substituting (15) into (16), the delay spread upper bound can be obtained based on the possible solutions of $\text{OP}_\mathbf{1}$ as

$$T_{\text{De}}^{\text{upp}}(t) = \max\{\tau_{p_0,q_0}(t) + \frac{\psi_{p_0,q_0}(t)}{2\pi f_c}, \max_{\tilde{p},\tilde{q}}\{\tau_{p_0,q_0}(t) + \frac{\zeta_{\tilde{p},\tilde{q}}(t)}{f_c} + \frac{\psi_{p_0,q_0}(t)}{2\pi f_c}\}\} - \min_{p,q}\{\tau_{p,q}(t)\}. \tag{17}$$

In the following, we minimize the objective function in $\text{OP}_\mathbf{2}$. Based on (15) and the causality requirement, $\psi_{p,q}(t) \geq 0$, we have

$$\zeta_{\tilde{p},\tilde{q}}(t) \geq -f_c\varpi_{\tilde{p},\tilde{q}}(t) - \frac{\psi_{p_0,q_0}(t)}{2\pi}, \tag{18}$$

from (18) and since $\zeta_{\tilde{p},\tilde{q}}(t) \in \mathbb{Z}$, the minimum value of $\zeta_{\tilde{p},\tilde{q}}(t)$ can be obtained as $\zeta_{\tilde{p},\tilde{q}}^{\min}(t) = \lceil -f_c\varpi_{\tilde{p},\tilde{q}}(t) - \frac{\psi_{p_0,q_0}(t)}{2\pi}\rceil$ which is a decreasing function with respect to $\psi_{p_0,q_0}(t)$. Equation (17) includes additional increasing function, i.e., $\frac{\psi_{p_0,q_0}(t)}{2\pi f_c}$. By substituting $\zeta_{\tilde{p},\tilde{q}}^{\min}(t)$ into (17), it is obvious that the variation of $\psi_{p_0,q_0}(t) \in [0, 2\pi]$ results in a small variation, less than $\frac{1}{f_c}$, in $T_{\text{De}}^{\text{upp}}(t)$. Hence, we relax $\zeta_{\tilde{p},\tilde{q}}^{\min}(t)$ to $\zeta_{\tilde{p},\tilde{q}}^{\text{R}}(t) = \lceil -f_c\varpi_{\tilde{p},\tilde{q}}(t)\rceil$, which turns (17) into an increasing function with respect to $\psi_{p_0,q_0}(t)$. Accordingly, the closed-form solution for the RIS phase shifts are obtained as (10) by considering $\psi_{p_0,q_0}(t) = 0$ and substituting $\zeta_{\tilde{p},\tilde{q}}^{\text{R}}(t)$ into (15). This closed-form solution is Pareto optimal based on [21, Th. 4.2.1]. Accordingly, (10) jointly optimizes (4) and (5), as the first priority order, and minimizes (16) as the second priority order. Another potential solution of OP is to reverse the priority order between $\text{OP}_\mathbf{1}$ and $\text{OP}_\mathbf{2}$. This reversed priority approach leads to non-efficient solution that is presented later in Section IV. ■

Corollary 1: With this Pareto optimal solution, the Doppler spread is zero, the maximum value for the instantaneous cascade channel gain is achieved as $\frac{P_{\text{R}}^{\max}(t)}{P_{\text{T}}} = |\sum_{p=1}^{P}\sum_{q=1}^{Q}\Gamma_{p,q}(t)|^2$, and the delay spread upper bound is

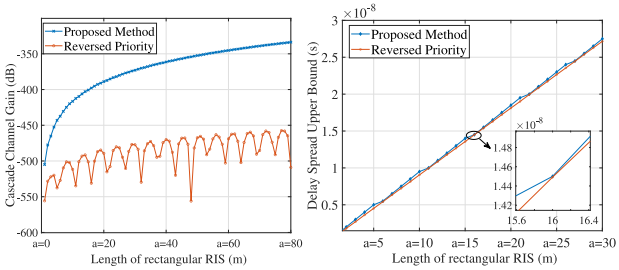

(a) (b)

Fig. 4. (a) Cascade channel gain versus RIS dimensions at $t = t_0$. (b) Delay spread upper bound versus RIS dimensions at $t = t_0$.

$$T_{\text{De}}^{\text{upp,min}}(t) = \max\{\tau_{p_0,q_0}(t), \max_{\tilde{p},\tilde{q}}\{\tau_{p_0,q_0}(t) + \frac{\zeta_{\tilde{p},\tilde{q}}^{\text{R}}(t)}{f_c}\}\} - \min_{p,q}\{\tau_{p,q}(t)\}. \tag{19}$$

As can be seen in Fig. 2, all the circular paths of the RIS elements have the same center located exactly between the Tx and Rx. With this symmetrical feature, the proposed closed-form solution works for all time slots due to the periodicity of the mobility patterns of the RIS elements.

IV. Numerical Evaluations

In this section, we evaluate the performance of our proposed RIS phase shift design in Section III. We assume a circular path with the origin (0, 0, 0) and the radius $R_0 = 3$ km parallel to xy-plane. The RIS dimensions are chosen in a way such that $a = 20 \times b$, i.e., the length is much larger than the width. This is because the RIS is mounted below the HAPS wing, as in Fig. 1. The RIS element dimensions are chosen as $d_x = d_y = \frac{\lambda_c}{5}$, where $f_c = 2$ GHz, and hence, the total number of RIS elements can be obtained as $P \times Q = \lceil\frac{a}{d_x}\rceil \times \lceil\frac{b}{d_y}\rceil = \lceil\frac{5a}{\lambda_c}\rceil \times \lceil\frac{a}{4\lambda_c}\rceil$. HAPS altitude and velocity of 20 km and $v = 110$ km/h are used in our simulations, respectively. These parameters are inline with the specifications of one of the well-known aerodynamic HAPS, HAWK30, [7], [22]. The terrestrial Tx and Rx coordinates in the scale of km are $(x_{\text{T}}, y_{\text{T}}, z_{\text{T}}) = (-5, 0, 20)$ and $(x_{\text{R}}, y_{\text{R}}, z_{\text{R}}) = (5, 0, 20)$, respectively. The planar antenna gain of RIS element (p, q) to S can be considered as $g_{p,q}^S(\theta_{p,q}^S(t), \varphi_{p,q}^S(t)) = \frac{4\pi}{\lambda_c^2} d_x d_y \cos\theta_{p,q}^S(t)$ for $\theta_{p,q}^S(t) \in [0, \frac{\pi}{2}]$ and zero otherwise, [13]. The gains of the transmit and receive antennas are $g_S^{p,q}(t) = 1$. As mentioned in *Lemma 2*, an alternative approach to our proposed method is optimization with reversed priority, i.e., reversing the order of $\text{OP}_\mathbf{1}$ and $\text{OP}_\mathbf{2}$ in the optimization process. Hence, in the following, we compare our proposed method with this alternative approach. In Fig. 4(a) and Fig. 4(b), the cascade channel gain and $T_{\text{De}}^{\text{upp}}(t)$ of the proposed method and reversed approach are compared at a snapshot $t_0 = 10$ s. Using the result of *Corollary 1*, in Fig. 4(a), we plot the cascade channel gain versus RIS dimensions. As can be seen, in Fig. 4(a), the reversed approach leads to a poor performance compared to our proposed method. Exploiting the proposed method makes the cascade channel gain controllable and it can be constructively increased by increasing the RIS dimensions. In contrast, the cascade channel gain based on reversed approach is uncontrollable as the only controllable parameter, i.e., the RIS phase shifts are fixed. This is due to the fact, mentioning in *Lemma 2*, that $\psi_{p,q}(t)$ is considered zero $\forall p, q, t$ to optimize $T_{\text{De}}^{\text{upp}}(t)$

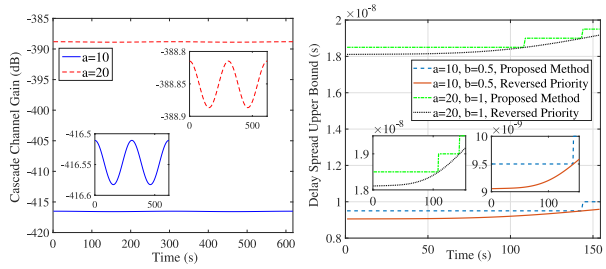

(a) (b)

Fig. 5. (a) Cascade channel gain versus time for different RIS dimensions. (b) Delay spread upper bound versus time for different RIS dimensions.

with the first priority order. By substituting $t = t_0$ s and zero phase shifts in (4), the cascade channel gain can be formulated as $\frac{P_{\mathrm{R}}(t_0)}{P_{\mathrm{T}}} = |\sum_{p=1}^{P}\sum_{q=1}^{Q}\Gamma_{p,q}(t_0)\exp(-j2\pi f_c\tau_{p,q}(t_0))|^2$. The term $\exp(-j2\pi f_c\tau_{p,q}(t_0))$ can negatively affect the cascade channel gain and makes it uncontrollable. Adopting the results of *Corollary 1*, in Fig. 4(b), we plot $T_{\mathrm{De}}^{\mathrm{upp}}(t_0)$ versus RIS dimensions to compare the proposed method and the reversed one. It can be seen that the delay spread gap between our proposed method and the reversed priority is negligible. Furthermore, by extrapolating Fig. 4(b), we can see that for $a = 80$ m, $T_{\mathrm{De}}^{\mathrm{upp}}(t_0)$ is around 8×10^{-8} s. This is due to the almost linear behavior of $T_{\mathrm{De}}^{\mathrm{upp}}(t_0)$ as a function of a. Therefore, (10) can keep the delay spread upper bound controllable even for a large number of RIS elements. The claims for Fig. 4(a) and Fig. 4(b) are feasible for any $t = t_0$ based on the results presented in Figs. 5(a) and 5(b). In Figs. 5(a) and 5(b), we analyze the cascade channel gain and $T_{\mathrm{De}}^{\mathrm{upp}}(t)$ versus time for different RIS dimensions, respectively. Fig. 5(a) shows that by increasing the value of a from 10 m to 20 m, the cascade channel gain can be increased by 27.7 dB. As can be seen, the fluctuation is less than 0.1 dB and can be ignored as it is negligible compared to the average value of the cascade channel gain. There is no significant benefit to consider the time-varying transmit signal to compensate this negligible fluctuation. In Fig. 5(b), we plot $T_{\mathrm{De}}^{\mathrm{upp}}(t)$ versus time to compare our proposed method with the reversed approach. As can be seen, the gap is less than 5×10^{-10} s and it is negligible. In addition, it is clear that (10) can make $T_{\mathrm{De}}^{\mathrm{upp}}(t)$ controllable for different time slots.

V. Conclusion

In this letter, we proposed a new network architecture exploiting an aerodynamic HAPS-RIS to provide connection between the unconnected ground stations. We proposed a multi-objective optimization problem for designing the RIS phase shifts based on the predictable mobility of aerodynamic HAPS-RIS. We found a closed-form solution for the RIS phase shifts, adopting Pareto optimality, based on an RIS reference element. We maximized the channel gain, forced the Doppler spread to zero, and minimized the delay spread upper bound. By exploiting this closed-form Pareto optimal solution, we do not need to constantly track the channel variations and constantly update the RIS phase shifts by solving optimization problems. Finally, we showed the performance efficacy of our proposed closed-form solution through numerical simulation.

References

[1] "Study on new radio to support non-terrestrial networks," 3GPP, Sophia Antipolis, France, Rep. TR 38.811, 2018. [Online]. Available: https://www.3gpp.org/ftp//Specs/archive.

[2] J. Ye, J. Qiao, A. Kammoun, and M.-S. Alouini, "Non-terrestrial communications assisted by reconfigurable intelligent surfaces," *Proc. IEEE*, vol. 110, no. 9, pp. 1423–1465, Sep. 2022.

[3] P. Ramezani, B. Lyu, and A. Jamalipour, "Toward RIS-enhanced integrated terrestrial/non-terrestrial connectivity in 6G," *IEEE Netw.*, early access, Aug. 1, 2022, doi: 10.1109/MNET.116.2200060.

[4] S. Alfattani et al., "Aerial platforms with reconfigurable smart surfaces for 5G and beyond," *IEEE Commun. Mag.*, vol. 59, no. 1, pp. 96–102, Jan. 2021.

[5] S. Alfattani, W. Jaafar, Y. Hmamouche, H. Yanikomeroglu, and A. Yongaçoglu, "Link budget analysis for reconfigurable smart surfaces in aerial platforms," *IEEE Open J. Commun. Soc.*, vol. 2, pp. 1980–1995, 2021.

[6] E. Björnson, Ö. Özdogan, and E. G. Larsson, "Intelligent reflecting surface versus decode-and-forward: How large surfaces are needed to beat relaying?" *IEEE Wireless Commun. Lett.*, vol. 9, no. 2, pp. 244–248, Feb. 2020.

[7] G. K. Kurt et al., "A vision and framework for the high altitude platform station (HAPS) networks of the future," *IEEE Commun. Surveys Tuts.*, vol. 23, no. 2, pp. 729–779, 2nd Quart., 2021.

[8] S. Alfattani, A. Yadav, H. Yanikomeroglu, and A. Yongacoglu, "Beyond-cell communications via HAPS-RIS," in *Proc. IEEE Globecom Workshops (GC Wkshps)*, 2022, pp. 1383–1388.

[9] S. Alfattani, A. Yadav, H. Yanikomeroglu, and A. Yongaçoglu, "Resource-efficient HAPS-RIS enabled beyond-cell communications," *IEEE Wireless Commun. Lett.*, vol. 12, no. 4, pp. 679–683, Apr. 2023.

[10] C. Pan et al., "An overview of signal processing techniques for RIS/IRS-aided wireless systems," *IEEE J. Sel. Topics Signal Process.*, vol. 16, no. 5, pp. 883–917, Aug. 2022.

[11] S. Sun and H. Yan, "Channel estimation for reconfigurable intelligent surface-assisted wireless communications considering Doppler effect," *IEEE Wireless Commun. Lett.*, vol. 10, no. 4, pp. 790–794, Apr. 2021.

[12] Z. Huang, B. Zheng, and R. Zhang, "Roadside IRS-aided vehicular communication: Efficient channel estimation and low-complexity beamforming design," Jul. 2022, *arXiv:2207.03157*.

[13] B. Matthiesen, E. Björnson, E. De Carvalho, and P. Popovski, "Intelligent reflecting surface operation under predictable receiver mobility: A continuous time propagation model," *IEEE Wireless Commun. Lett*, vol. 10, no. 2, pp. 216–220, Feb. 2021.

[14] W. Wu, H. Wang, W. Wang, and R. Song, "Doppler mitigation method aided by reconfigurable intelligent surfaces for high-speed channels," *IEEE Wireless Commun. Lett.*, vol. 11, no. 3, pp. 627–631, Mar. 2022.

[15] Z. Huang, B. Zheng, and R. Zhang, "Transforming fading channel from fast to slow: Intelligent refracting surface aided high-mobility communication," *IEEE Trans. Wireless Commun.*, vol. 21, no. 7, pp. 4989–5003, Jul. 2022.

[16] B. Zheng, S. Lin, and R. Zhang, "Intelligent reflecting surface-aided LEO satellite communication: Cooperative passive beamforming and distributed channel estimation," *IEEE J. Sel. Areas Commun.*, vol. 40, no. 10, pp. 3057–3070, Oct. 2022.

[17] Ö. Özdogan, E. Björnson, and E. G. Larsson, "Intelligent reflecting surfaces: Physics, propagation, and pathloss modeling," *IEEE Wireless Commun. Lett.*, vol. 9, no. 2, pp. 581–585, May 2020.

[18] E. Björnson, H. Wymeersch, B. Matthiesen, P. Popovski, L. Sanguinetti, and E. Carvalho "Reconfigurable intelligent surfaces: A signal processing perspective with wireless applications," *IEEE Signal Process. Mag.*, vol. 39, no. 2, pp. 135–158, Mar. 2022.

[19] H. T. Friis, "A note on a simple transmission formula," *Proc. IRE*, vol. 34, no. 5, pp. 254–256, 1946.

[20] E. Björnson, E. A. Jorswieck, M. Debbah, and B. Ottersten, "Multiobjective signal processing optimization: The way to balance conflicting metrics in 5G systems," *IEEE Signal Process. Mag.*, vol. 31, no. 6, pp. 14–23, Nov. 2014.

[21] K. Miettinen, *Nonlinear Multiobjective Optimization*, vol. 12. Boston, MA, USA: Springer, 1999.

[22] "HAPSMobile." Accessed: Nov. 24, 2022. [Online]. Available: https://www.hapsmobile.com/